Received: 12 February 2024 | Revised: 2 December 2024 | Accepted: 3 December 2024

DOI: 10.1002/ar.25623

SPECIAL ISSUE ARTICLE

The Anatomical Record WILEY

Only skull-deep? Headbutting adaptations may not extend to the brain cavity

Nicole L. Ackermans[1,2] | **Joy S. Reidenberg**[3]

[1]College of Arts and Sciences, Department of Biological Sciences, University of Alabama, Tuscaloosa, Alabama, USA

[2]Clinic for Zoo Animals, Exotic Pets and Wildlife, Vetsuisse Faculty, University of Zurich, Zürich, Switzerland

[3]Center for Anatomy and Functional Morphology, Icahn School of Medicine at Mount Sinai, New York, New York, USA

Correspondence
Nicole L. Ackermans, College of Arts and Sciences, Department of Biological Sciences, University of Alabama, Tuscaloosa, Alabama, USA.
Email: nlackermans@ua.edu

Funding information
Schweizerischer Nationalfonds zur Förderung der Wissenschaftlichen Forschung, Grant/Award Number: P2ZHP3_191255

Abstract

High-impact headbutting behavior makes the muskox (*Ovibos moschatus*) a charismatic species. While many theorize how these headbutting bovids might protect their brain during such encounters, few have investigated their claims anatomically. We investigated the anatomical function of digitiform impressions in the bovid brain cavity and their relationship to headbutting. This work is divided into two parts. First, we provide an anatomical description of the muskox brain cavity for the first time in literature. We used computed tomography (CT) scans of adult and juvenile muskoxen skulls and scans of a goat (*Capra hircus*) skull for comparison. As the texture of the muskox brain cavity appeared pronounced, we sought to quantify the digitiform impressions that create this rough appearance, with the hypothesis that they support the brain and reduce injury during headbutting. We developed a simple measurement to quantify digitiform impressions called the endocranial roughness index (ERI). In the second part of this work, the ERI was applied to a sample of 59 headbutting and non-headbutting bovid species. Contrary to our expectations, the quantitative assessment of digitiform impressions across various taxa revealed no correlation between endocranial roughness and headbutting. We conclude that endocranial roughness either only affects brain protection at a smaller scale, or endocranial roughness at the measured scale does not have an effect on brain protection significant enough to cause selective evolutionary pressure.

KEYWORDS

bovid, braincase, concussion, skull, traumatic brain injury

1 | INTRODUCTION

Within Bovidae, the only species that truly headbutt are in the Caprinae subfamily: sheep, goats, and muskoxen. Of those, muskoxen (*Ovibos moschatus*) are one of the most extreme, headbutting at high forces due to their large mass and high collision speeds. While it is safe to assume that a thick skull and large horns mitigate injury from skull fractures, little is known about anatomical contributions protecting the brain from severe trauma. Recent work from our group found evidence of chronic brain injury in both male and female muskoxen (Ackermans et al., 2022), indicating that whatever protection does exist is not absolute. In this publication we will provide first an anatomical description of the muskox's brain cavity, and second, an analysis of the relationship between brain cavity surface texture (endocranial roughness) and headbutting behavior.

 © 2025 American Association for Anatomy.

Muskoxen are easily recognized by their helmet-shaped horns, with broad bases and recurved points adapted for a ramming style of fighting (Emlen, 2008; Lönnberg, 1901; Lundrigan, 1996; Opdam et al., 2002). Female muskoxen have smaller horns than males, with narrower horn bases and less fusion along the dorsal midline (Smith, 1976). During extended fights, muskox bulls may experience more than 20 repetitive clashes (Gray, 1973; Smith, 1976), with some dominant animals undergoing over 100 high-force impacts in a few months (Gray, 1973). Bulls will rush toward each other at a full gallop, up to 27 km/h (Smith, 2008), and strike heads on their wide horn bases (Smith, 1976). These speeds, combined with the average weight of adult muskox (approximately 120–320 kg for bulls, and 90–200 kg for cows (Thing et al., 1987)) produce impact forces of around 225 kN, equivalent perhaps to experiencing a car crash at 56 km/h (35 mph). The head-on clashes are usually followed by pushing, jabbing, and hooking of sharp horns, sometimes resulting in serious goring injuries (Smith, 1976). Surprisingly, these annual combat events result in a low frequency of deaths, roughly estimated at 5%–10% (Wilkinson & Shank, 1976), although a harsh winter in addition to an exhausting rut can increase fatalities (Gunn et al., 1989). Deaths are not generally directly attributed to headbutting, although Smith (1976) observed bulls "often acting dazed" after combat, as well as some animals bleeding from the nose and ears after fighting for several days (an injury also observed in three carcasses by Wilkinson and Shank (1976)). Note that while bleeding can be caused by skull fracture, it may also be caused by injuries from horn impalement or parasitic infection (yersinosis), common in muskoxen (Blake et al., 1991).

It had long been assumed that muskoxen were immune to brain injury caused by headbutting, but that claim lacks both data and an understanding of the selective pressures of evolution (Ackermans, 2023). Although the literature is sparse, female muskoxen are reported to participate in headbutting to establish a social hierarchy, at least in captivity (Gray, 1973; Ihl & Bowyer, 2011) (pers. Comm. Jamie Luce Muskox Ox Farm, AK). However, female muskox headbutting behavior does not seem to have as strong as a selective effect on skull anatomy as in males. The male muskox skull is about 300% heavier than the female skull (Smith, 1976), with the male's skull covered by around 10 cm of horn on top of 8 cm of pneumatized cranial bone (Figures 1b and 2a). A large head and horns are an external signal of fitness to other competing males and selecting females, and may also contribute some external protection. However, a thick skull alone may not protect the brain from the inside, where a sudden impact might cause the brain to shift and repeatedly hit the walls of the brain cavity, creating a concussion. No specific factors contributing to brain protection have been empirically identified in headbutting animals, despite in-depth biomechanical studies on skull and horn structure (Aguirre et al., 2020; Wheatley et al., 2023), as well as postcranial elements (Schüler et al., 2024; Vander Linden & Dumont, 2019). Some hypothesize that heavily pneumatized sinuses are the main contributors to impact-force mitigation in headbutting bovids (for a review of the history of headbutting theories in the literature, see this special issue, Ackermans et al., 2024), but a study on domestic goats showed no difference in force absorption between goat skulls modeled with or without large frontal sinuses (Farke, 2008). Most likely, pneumatized cranial bones and horn cores are not strictly protective but have several other functions, including thermoregulation (Picard et al., 1994; Picard et al., 1999; Taylor, 1966), weight reduction without loss of stability (Preuschoft & Witzel, 2002), and scaffolding for rapid horn growth (Farke, 2008). The interior of the skull and its relationship to headbutting behavior is even less understood than its exterior. Our hypothesis was that the roughness of the brain cavity contributes to brain stabilization during impact.

Endocranial roughness develops during vertebrate neurocranial development, aligning approximately with the gyri and sulci of the brain in many species. These impressions have also been called endocranial imprints (Zollikofer & De León, 2013), convolutional patterns (Clark et al., 1936; Darlington, 1957), mammillary eminences (Peña-Melián et al., 2011), or digitiform impressions (*impressiones digitae*) (Schaller & Constantinescu, 2007).

Published anatomical measurements and descriptions for muskoxen include: oral anatomy (Mathiesen et al., 2000), tooth wear (Fortelius & Solounias, 2000), gross cranial morphology (Lent, 1988; Márquez et al., 2017; Smith et al., 2002), brain mass (Kopperud, 2017; Pérez-Barbería & Gordon, 2005), as well as cranial measurements on fossil, remains (Brand et al., 2020; Harington, 1970; Kitts, 1953; Krakhmalnaya & Kovalchuk, 2018; Skwarawoolf & Millar, 1981; Stefaniak et al., 2021; Walker, 1982) (for a review of recent and fossil specimen measurements, see Stefaniak et al., 2021). However, the brain cavity (i.e., the endocranial surface of the skull) has not been anatomically described for this species, likely due to limits on destructive analysis of such rare material. A modern solution to non-destructive anatomical examination is the use of digital imaging such as computed tomography (CT) scans to visualize skeletal and soft tissue elements. We therefore offer a detailed description of the muskoxen brain cavity in this study, focusing on the textured surface (endocranial roughness) as visualized in CT scans. In the first part of this publication, we compare and describe brain cavity anatomy in detail using CT scans of the skulls of four adults and two juvenile muskoxen, as well as one adult goat (*Capra hircus*). In the second part of this publication, we develop the endocranial

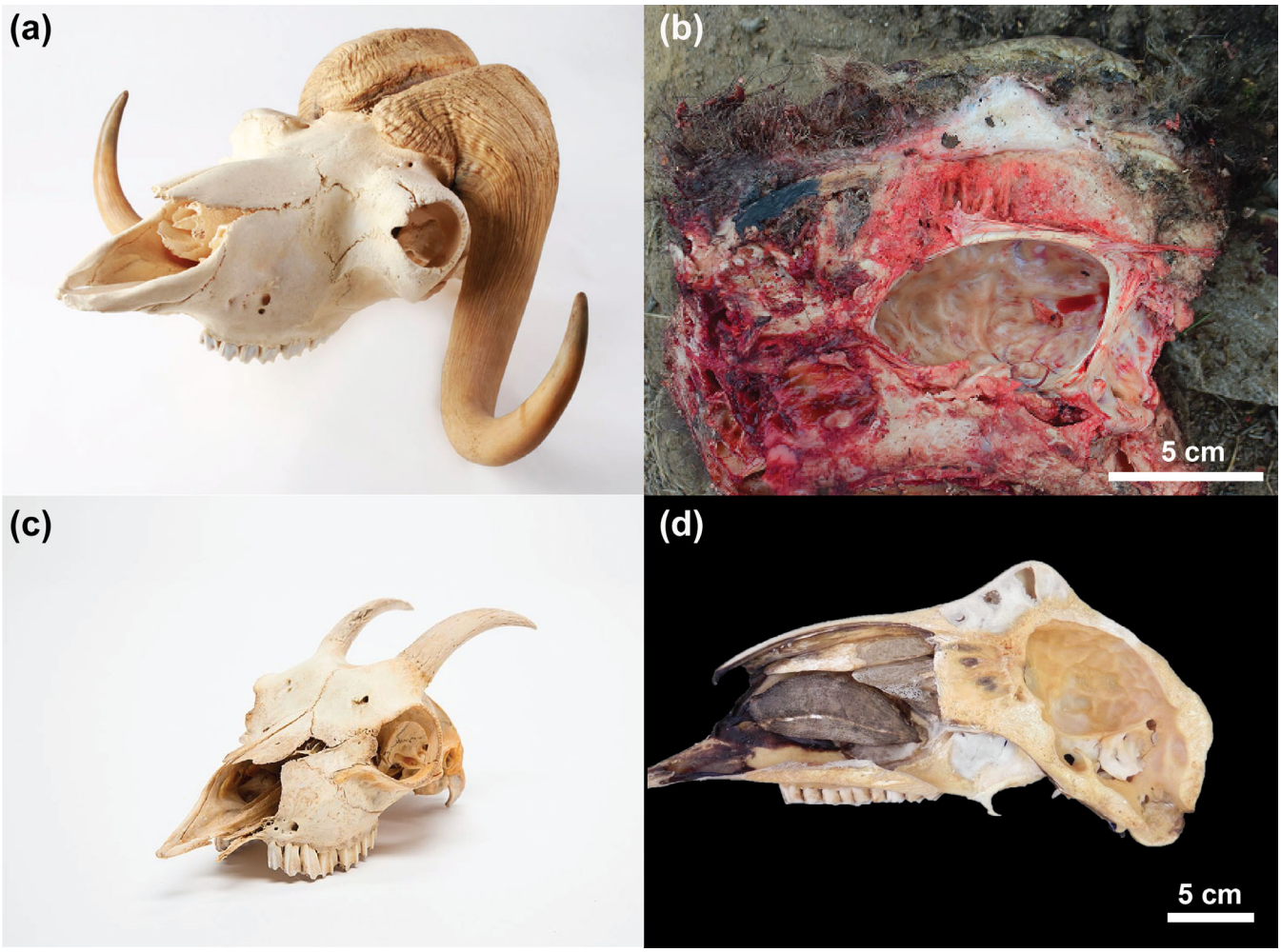

FIGURE 1 Skull and brain cavity of muskox (*Ovibos moschatus*) and goat (*Capra hircus*). (a) Muskox skull, *Source*: Wikimedia Commons. (b) Brain cavity of a Muskox skull with the dura mater intact, *Source*: Terrie Williams. (c) Goat skull, *Source*: Wikimedia Commons. (d) Brain cavity of a goat skull. Scalebar = 5 cm.

roughness index (ERI) to quantify endocranial ridges visualized in CT scans and photographs of bisected dry bone skulls in 59 bovids, including both headbutting and non-headbutting species. Our aim was to determine whether a high degree of ERI and thus a large quantity of pronounced ridges, is linked to headbutting behavior.

2 | MATERIALS AND METHODS

2.1 | Specimens used for anatomical description

Muskox (*O. moschatus*) specimens (see Table 1) comprise six CT-scanned skulls. Two whole head CT scans of juvenile specimens include IZW 542/2001 (juvenile male, cause of death (COD): enteritis, origin: zoo) and IZW 213/1997 (neonate male, COD: stillborn, with atelectasis of the lungs, origin: zoo) from Tierpark Berlin, previously used to describe larynx anatomy in Frey et al. (2006). The four adult male skull CT scanned specimens include AMNH 29949 (origin: wild) and AMNH 800095 (origin: zoo) from the American Museum of Natural History, previously used to describe sinus anatomy in Farke (2010), as well as UCMZ 1978.1.92 (origin: zoo) and UCMZ 1979.60 (origin: wild) from the University of Calgary Museum of Zoology, previously used to describe headbutting anatomy in Snively and Theodor (2011). A domestic goat (*Capra hircus*) AMNH 88691 (adult male) was used for comparison. Note that the adult specimens in this collection are male, as female muskoxen are rarely part of museum collections that were often acquired during trophy hunting excursions. Although some of these specimens were sourced from the wild, trophy specimens may not be representative of an average population (Coltman et al., 2003; Cooper et al., 2019), however, they represent an extreme of sexual dimorphism. Anatomical descriptions are provided for the skull and brain cavity of muskoxen based on CT scans. Anatomical terms follow the Nomina Anatomica

TABLE 1 Specimens used to score endocranial roughness index.

Species	Common name	Museum ID	Headbutt	Weight (kg)
Aepyceros melampus	Impala	YPM3982	N	62.5
Alcelaphus buselaphus	Hartebeest	HBEAST14572	N	172
Antidorcas marsupialis	Springbok	AMNH165080	N	29
Antilocapra americana	Pronghorn	YPM1513	N	52
Antilope cervicapra	Blackbuck	AMNH19613, 54486	Y	35
Bison bison	Bison	YPM3406	Y	730
Bos javanicus	Banteng	AMNH113755	N	700
Boselaphus tragocamelus	Nilgai	AMNH22842, 35520, YPM234, 5224	N	245
Bubalus depressicornis	Lowland anoa	AMNH61146, 152856, 152,864	N	225
Bubalus mindorensis	Tamaraw	AMNH40046	N	237
Budorcas taxicolor	Takin	AMNH110477	Y	250
Capra falconeri	Markhor	AMNH54610	Y	96.5
Capra hircus aegagrus	Wild goat	AMNH88691, 88697	Y	92
Capra ibex sibirica	Siberian ibex	AMNH54906, 57317	Y	95
Cephalophus dorsalis	Bay duiker	AMNH52917, 52924, 52,987	N	21
Cephalophus leucogaster	White-bellied duiker	AMNH52799, 52802, 52804, 52843	N	17.5
Cephalophus natalensis	Red forest duiker	AMNH216375	N	13.5
Cephalophus niger (maxwelli)	Black duiker	AMNH89402, 89432, 89625	N	21
Cephalophus nigrifrons	Black-fronted duiker	AMNH52942, 52949, 52951, 52989, 52978	N	15.5
Cephalophus sylvicultor	Yellow-backed duiker	AMNH170368, 55382, 55383	N	62.5
Connochaetes taurinus	Blue wildebeest	YPM3922, 3970, 5119	N	263.5
Damaliscus lunatus	Tsessebe	YPM3867, 3971, 5117	N	130
Gazella dorcas	Dorcas gazelle	AMNH82288	N	16.5
Gazella subgutturosa	Goitered gazelle	AMNH57272, 57263	N	25.5
Gazella thomsonii	Thomson's gazelle	YPM3631, 4042, 6068	N	27.5
Hemitragus hylocrius	Nilgiri tahr	AMNH54755, YPM1504	Y	75
Hippotragus equinus	Roan antelope	YPM3524	N	267.5
Hippotragus niger	Sable antelope	AMNH83606, YPM3523	N	220
Kobus ellipsiprymnus	Waterbuck	YPM3484, 3566, 3576	N	262.5
Kobus leche	Lechwe	YPM14577	N	111.5
Kobus vardoni	Puku	YPM3366	N	79
Litocranius walleri	Gerenuk	YPM5115, 3987, AMNH81170	N	40
Madoqua	Dik-dik	YPM3985, 5462, 9485	N	4.5
Naemorahedus goral	Himalayan goral	AMNH43033, 110485	Y	38.5
Naemorahedus sumatraensis	Mainland serow	AMNH45348, YPM1511	Y	37.5
Neotragus batesi	Bates's pygmy antelope	AMNH53192, 53169	N	2.5
Neotragus moschatus	Suni	YPM2993, 3129	N	4.5
Oreamnos americanus	Mountain goat	YPM14605, AMNH60793	N	112.5
Oreotragus oreotragus	Klipspringer	YPM5112, 2992, AMNH27827	N	10.5
Oryx gazella	Gemsbok	AMNH233035	N	237.5
Ourebia ourebia	Oribi	YPM1502, AMNH90163	N	13.5

TABLE 1 (Continued)

Species	Common name	Museum ID	Headbutt	Weight (kg)
Ovibos moschatus	Muskox	AMNH29949, 80095, UCMZ1978.1.92, 1979.60, IZW542/2001, 293/1997	Y	295
Ovis ammon	Argali	YPM4295	Y	138
Ovis canadensis	Bighorn sheep	YPM183, 1489, 1490	Y	112.5
Pantholops hodgsonii	Tibetan antelope	AMNH55819, YPM14610	N	37.5
Pelea capreolus	Gray rhebok	YPM1499	N	24
Procapra gutturosa	Mongolian gazelle	AMNH57260, 85235	N	29.5
Pseudois nayaur	Bharal	AMNH117401, 110494	Y	67.5
Raphicerus campestris	Steenbok	AMNH54186, 54193	N	11
Redunca arundinum	Southern reedbuck	YPM3563	N	77.5
Redunca fulvorufula	Mountain reedbuck	AMNH54257, YPM3979	N	29.5
Rupicapra rupicapra	Chamois	AMNH90237	Y	38
Saiga tatarica	Saiga antelope	YPM1510	N	36
Sylvicapra grimmia	Common duiker	YPM5832, 9433	N	18.5
Syncerus caffer	African buffalo	YPM3612	N	700
Taurotragus oryx	Common eland	YPM4087, 6059	N	700
Tetracerus quadricornis	Four-horned antelope	ANMH54941, 54983, YPM1509	N	20
Tragelaphus scriptus	Harnessed bushbuck	BUCK1, 2, 3	N	60
Tragelaphus strepsiceros	Greater kudu	NA	N	217.5

Note: Dataset provided by Andrew Farke. Y = yes, N = no.

Veterinaria (International Committee on Veterinary Gross Animal Nomenclature, 2017). The endocranial surface of the brain cavity was examined through 3D renderings of CT scan images.

2.2 | CT

Specimen IZW 542/2001 was scanned using a GE Light Speed QX/I Spiral scan, at 1.25 mm slice thickness at 120 kV and 200 mA. Specimen IZW 213/1997 was scanned with a GE Light Speed QX/I Spiral scan, at 1.25 mm slice thickness at 120 kV and 160 mA. All AMNH and YPM specimens were scanned using a GE Lightspeed 16 CT scanner at various slice thicknesses and at 100 kVp, using the BONE-LPUS convolution kernel. The voxel size for each scan is reported in the Supplementary Information, using the formula (pixel spacing * pixel spacing * slice thickness).

2.3 | Endocranial Roughnes Index

ERI was determined from a dataset compromising CT scans of 59 bovid species. All CT scanned specimens were male. For species with multiple individuals, we scored all of them and averaged the score per species. ERI was scored between 0 (smooth) and 15 (rough). The bovid CT scan dataset was provided by Andy Farke (Farke, 2008, 2010). Skulls were rendered in 3D and bisected in the midline using Horos software (Horos v3.3.6). Species used in this study were determined by the availability of CT scans and skulls in our and collaborators' collections (see Table 1 for specimen list and sources).

ERI was measured by observers who were either trained anatomists ($n = 2$) or untrained students ($n = 4$) and blinded to species to reduce bias and interobserver variation. Participants were asked to count the number of endocranial ridges intersecting with a red line drawn approximately vertically from the presphenoidal synchondrosis (if ossified or not present, we used the anterior edge of the pituitary fossa) to the craniometric point bregma (intersection of frontal and parietal bones); and then to count the number of endocranial ridges intersecting with a blue line drawn approximately horizontally from the superior or rostral edge of the cribriform plate to confluence of sinuses (if not visible, we used the cerebrum-cerebellum separation where the tentorium attaches or the craniometric point lambda where the

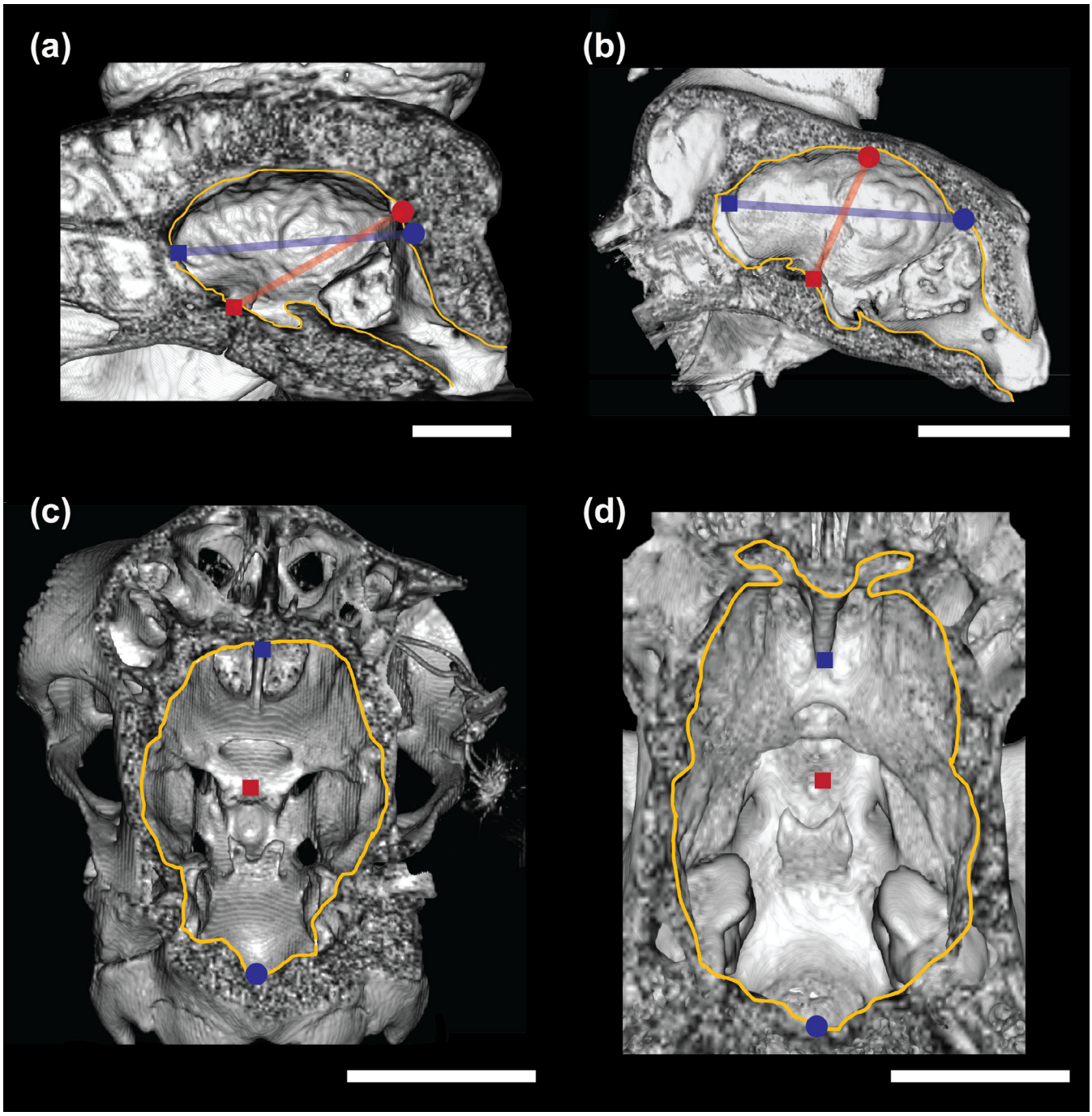

FIGURE 2 Comparison of muskox (*Ovibos moschatus*) and goat (*Capra hircus*) brain cavities through computed tomography scans. (a) Muskox, midsagittal plane; (b) Goat, midsagittal plane; (c) Muskox, dorsal plane; (d) Goat, dorsal plane. Orange outlines are a visual guide to represent the section of the visible brain cavity within the CT scan image. Images a) and b) show a midsagittal plane through the cranium with the rostrum facing toward the left. Images c) and d) show a dorsal view of a horizontal plane through the cranium, with the rostrum facing the top of the image. The red and blue points indicate landmarks used to draw each line for endocranial roughness index (ERI) scoring. Blue square = superior rostral edge of the cribriform plate, blue circle = confluence of sinuses or cerebrum/cerebellum separation, red square = anterior edge of the pituitary fossa or presphenoidal synchrondrosis, red circle = craniometric point bregma. Images represent the skulls alone, with no brain tissue present. The goat is specimen AMNH88691, the muskox is specimen UCMZ1978.1.92. Scalebar = 5 cm.

occipital bone meets the parietal bones) (Figure 2). If any endpoint was missing due to skull damage ($n = 2$), the vertical approximation for the blue line was taken perpendicular to the hard palate in the vertical plane, and the horizontal approximation for the red line was taken parallel to the hard palate in the horizontal plane,

and endocranial roughness was measured for the portions of the skull covered by the lines traversing up to the breakage points. ERI was calculated as follows: blue line count + red line count averaged across all observers per species. Images provided to participants for scoring and raw scores are provided in the Supplementary Information.

2.4 | Statistical analysis

All statistical analysis was performed using R Statistical Software (R Core Team, 2021). We defined headbutting behavior as clashing head-to-head in combat, eliminating head-to-flank and non-clashing head-to-head pushing (Woodruff & Ackermans, 2024). Evidence of headbutting behavior in each species was sourced from the literature (Corlatti et al., 2013; Lovari et al., 2020; Lovari & Apollonio, 1994; Vander Linden & Dumont, 2019). Voxel size was calculated from slice thickness and pixel spacing associated with each CT scan and used as an indicator for CT resolution. Additionally, animal average weights were reported, as a measure of overall size (Castelló, 2016).

Voxel size and ERI score were averaged by species and tested for normality using a Shapiro–Wilk normality test. Data was made categorical, to test correlations with Pearson's Chi-squared tests with Yates continuity correction. Chi-squared test effect size was calculated using Cramer's V. Factors were considered independent when $p > 0.05$. The following factors were compared: headbutting behavior (yes/no) to ERI category; ERI category to voxel size (low/medium/high/very high); and voxel size to animal weight (low/medium/high/very high), when applicable. The same analyses were applied to a subgroup consisting of only species weighing on average more than 60 kg ($n = 29$), to eliminate size-related skewing. Annotated R code and raw data are available on GitHub: https://github.com/NLAckermans/2024ERI.git.

3 | RESULTS

3.1 | Anatomical description of the muskox brain cavity

As in other artiodactyls, the muskox brain cavity is made up of the frontal, parietal, occipital, temporal, sphenoid, and ethmoid bones, although in the neonate and juvenile, the basisphenoid and presphenoid bones are still separate as the intersphenoidal synchondrosis between them has not yet ossified. The inner surface of the brain cavity is rough, with a high number of bony crests and depressions (Figures 1 and 2). These are much less prominent in the neonate, especially ventrally (Figure 3). Most vascular impressions are not visible at the resolution of the CT scans obtained. The cranial vault (*calvaria*) consists of an external plate (*lamina externa*) and an internal plate (*lamina interna*) sandwiching the frontal sinuses (*sinus frontalis*) in between them. The neonate lacks most pneumatization of the frontal, parietal, and occipital bones (slightly more pneumatized in the juvenile), resulting in external and internal lamina that follow each other much more closely (Figure 3). In these juvenile muskoxen, there are no fontaneles (membrane coverings) between the bones. The caudal frontal sinus (*sinus frontalis caudalis*) is composed of solid bone in the muskox (Figures 1b and 2a). The large left and right frontal sinuses mainly pneumatize the cranial vault from the rostral edge of the orbits up to the rostral third of each horn's cornual process (*processus cornualis*). The neonate lacks osseous horn cores and sheaths altogether.

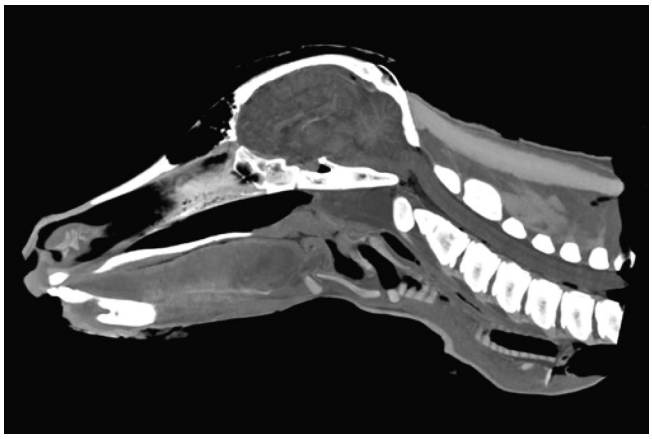

FIGURE 3 Computed tomography scan of a juvenile muskox (*Ovibos moschatus*) specimen. Rostrum pointing left, midsagittal section. Note the position of the brain inside the brain cavity. MRI scan courtesy of Roland Frey and Guido Fritch of the Leibniz Institute for Zoo and Wildlife Research Berlin.

3.1.1 | Rostral cranial fossa

The ventral aspect of muskox skull's brain cavity is described using a dorsal endocranial view after performing 3-D rendering and virtually sectioning in a horizontal plane (Figure 2). The most rostral cranial fossa extends medially from the cribriform plates (*laminae cribrosae*) to the orbitosphenoidal crest (*crista orbitosphenoidalis*), and laterally between the wings of the presphenoid bone (*alae ossis presphenoidalis*). The cribriform plates of the ethmoid bone (*lamina cribrosa ossis ethmoidalis*) are non-ossified in the neonate, almost completely ossified in the juvenile, and fully ossified in the adult. They are divided

by the perpendicular plate (*lamina perpendicularis*), that extends caudally into the cranial cavity as a sagittal crest (*crista galli*) that anchors the connective tissue separation between the cerebral hemispheres (*falx cerebri*). It also separates the paired ethmoid fossae (*fossae ethmoidales*). The ethmoidal foramen (*foramen ethmoidale*) lies rostrodorsal to the optic canal (*canalis opticus*) in the orbit. Beneath the orbitosphenoidal crest is the chiasmatic groove (*sulcus chiasmatis*).

3.1.2 | Central cranial fossa

The central cranial fossa of the Muskox skull extends rostral to caudal from the presphenoid bone to the crest (*cristae partis petrosae*) of the petrous portion of the temporal bone (*pars petrosa ossis temporalis*) and is characterized by the *sella turcica*, formed by the dorsal part of the basisphenoid bone (*dorsum sellae*) in the midline. The round foramen (*foramen orbitorotundum*) is situated lateral to the optic canal, while the oval foramen (*foramen ovale*) perforates the greater wing of the basisphenoid bone, lateral to the sella turcica and rostral to the petro-occipital fissure (*fissura petrooccipitalis*).

3.1.3 | Caudal cranial fossa

The caudal cranial fossa of the muskox skull extends rostra-caudally from the crest of the petrosal bone to the large opening for the brainstem and spinal cord (*foramen magnum*). The dorsal surface (*pars basilaris*) of the basioccipital bone shows two slight depressions on the ventral part, a shallower rostral impression (*impressio pontina*) and a deeper caudal impression (*impressio medullaris*). The basilar part of the occipital bone is separated from the petrosal part by the narrow petro-occipital fissure (Figure 2). Laterally, the cerebellar fossa is vaguely delineated from the cerebral fossa by a weak crest on the medial aspect (*facies medialis*) of the petrosal bone. The petrosal part and the tympanic part of the temporal bone accommodate the inner ear and the middle ear respectively. Dorsally adjacent to that crest is the opening of the internal acoustic meatus (*porus acousticus internus*), from where the short inner acoustic canal (*meatus acousticus internus*) runs laterally into the petrosal bone. The internal acoustic meatus is located posteriorly on the inner surface of the cranial cavity, close to the dorsal tip of the petrosal bone. The transverse crest (*crista transversa*) at the bottom of the internal acoustic meatus (*fundus meatus acustici interni*) is surrounded by four sub-fossa openings connecting to the inner ear. Ventral to the opening of the internal acoustic meatus, between the petrosal bone and the basioccipital bone, lies the jugular foramen. The lateral part of the occipital bone is perforated by a canal (*canalis nervi hypoglossi*).

Caudal to the temporal meatus lies the internal occipital protuberance, opposite a prominent, dorsoventrally oriented external occipital protuberance on the outer surface of the skull. The internal occipital protuberance is at the center of the cruciform eminence, which is formed by the junction of the two crests separating the large cranial cavity (*fossa cerebralis*) superiorly or rostrally from the small cranial cavity (*fossa cerebellaris*) inferiorly or caudally.

The dura is not clearly visible at CT scan resolution. The foramen magnum is formed by the occipital bone that is divided into the flat or squamous part (*squama occipitalis*) dorsally, the paired lateral parts (*pars lateralis*), and the basilar part (*pars basilaris*). The occipital condyles on the outer surface of the foramen magnum derive from the lateral parts of the occipital bone. They are integrated into the skull contour in the neonate, juvenile, and adult and are extremely massive in muskoxen.

Additional differences noted between the adult, juvenile, and neonate muskoxen in skeletal anatomy include the proportion of the neurocranium to the viscerocranium; this is about 1:1 in the newborn, 1:3 in the juvenile, and about 1:2 in an adult (Figures 1–3). In the neonate, the zygomatic arches are much closer to the skull surface and the temporal fossa is narrower. The neonate's orbits are not extended laterally, as is the case for the diagnostic orbits of the adult muskox skull. However, they are slightly more extended in the juvenile. The ventral arch of the atlas has not yet fused with its dorsal arch in the neonate but is fused in the juvenile, and the dens are still separate from the axis in the neonate but connected in the juvenile. While not a skeletal element, a frontal fat pad is lacking on the forehead in both young animals.

3.1.4 | Statistical analysis

Results from statistical analyses comparing ERI of different bovid species ($n = 59$) are presented in Table 2. Shapiro–Wilk normality tests showed that mean voxel size and weight were not normally distributed ($p = 1.642\text{e-}6$ and $p = 2.253\text{e-}10$, respectively), but that mean ERI scores showed a normal distribution ($p = 0.698$). As all factors were not normally distributed and some included small sample sizes, chi-squared was selected to test for coarse associations. Therefore, voxel size, weight, and ERI score were divided into categorical variables. All analyses were applied to either all species together ($n = 59$) or a subset of two groups: species > 60 kg ($n = 29$) or species < 60 kg ($n = 28$).

TABLE 2 Statistical independence between factors tested in this study.

	Factor 1	Factor 2	Test	*p*	W	df	Cramer's V
All species	Mean voxel size	Density	Shapiro–Wilk	1.64E-06	0.827		
	Animal weight	Density	Shapiro–Wilk	2.25E-10	0.651		
	Mean ERI score	Density	Shapiro–Wilk	0.698	0.985		
	Headbutting category	ERI category	Pearson's Chi-squared test with Yates' continuity correction	0.124	2.368	1	0.16
	Voxel size category	ERI category	Pearson's Chi-squared test	0.001	15.886	3	0.49
	Voxel size category	Weight category	Pearson's Chi-squared test	2.20E-16	165	9	1.00
<60 kg	Headbutting category	ERI category	Pearson's Chi-squared test with Yates' continuity correction	0.483	0.491	1	0.00
	Voxel size category	ERI category	Pearson's Chi-squared test	0.154	3.736	2	0.25
>60 kg	Headbutting category	ERI category	Pearson's Chi-squared test with Yates' continuity correction	0.755	0.097	1	0.00
	Voxel size category	ERI category	Pearson's Chi-squared test	0.025	9.368	3	0.50
	Voxel size category	Weight category	Pearson's Chi-squared test	0.886	2.338	6	0.00

Abbreviation: ERI, Endocranial Roughness Index.

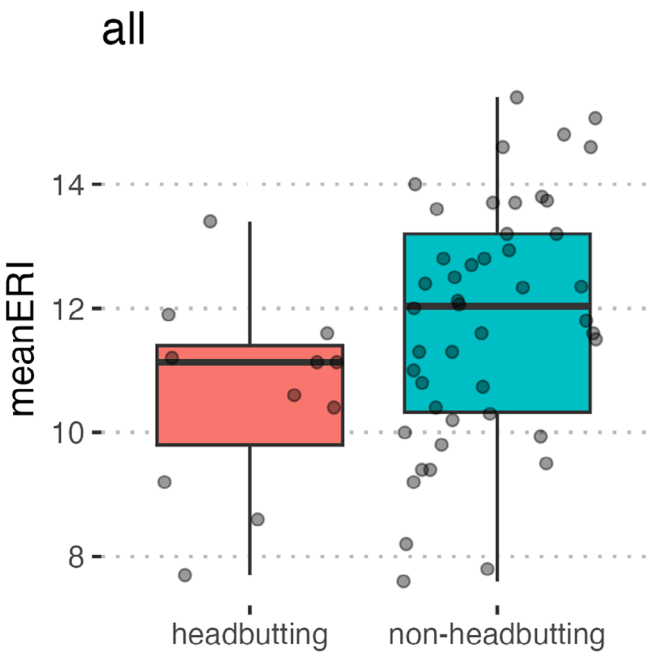

FIGURE 4 Boxplot comparing headbutting behavior to endocranial roughness index (ERI). ERI was scored on a dataset of 59 bovid species, all specimens were CT scans of adult male skulls. A low ERI (0) indicates a smooth brain cavity while a high ERI score (15) indicates a rough brain cavity. Headbutting species $n = 14$, non-headbutting species $n = 45$.

Results showed that headbutting behavior was independent of ERI category ($p = 0.124$, $X^2 = 2.369$, $V = 0.16$) (Figure 4). This remained true when considering both small and large animals, at $p = 0.483$, and $p = 0.755$, respectively, with Cramer's $V = 0$ for both indicating a weak relationship.

ERI category was independent of voxel size ($p = 0.001$, $X^2 = 15.71$, Cramer's $V = 0.49$) when considering all species, but dependent on voxel size for smaller animals ($p = 0.187$, $X^2 = 3.736$, Cramer's $V = 0.25$). In larger animals while significant ($p = 0.059$, $X^2 = 9.368$), Cramer's $V = 0$ indicates no strong correlation between variables. Voxel size was dependent on animal weight for all species ($p = 0.345$, $X^2 = 165$, Cramer's $V = 1$), but showed no strong association in the larger animals ($p = 0.886$, $X^2 = 2.338$, Cramer's $V = 0$). Annotated R code is available on GitHub.

4 | DISCUSSION

4.1 | Anatomical description

The use of CT scans in this work allowed noninvasive visualization of the surface anatomy of the interior of the muskoxen skull. This is the first description of the muskox brain cavity in peer-reviewed literature.

Overall, muskoxen skulls have a proportionally larger ethmoid fossa than goats. Adult domestic goats are approximately a third of the size of adult muskoxen and in the goat specimen, the brain cavity volume was about half of that of the average volume for the muskoxen, although the general shape was similar. There were some

notable differences in muskox endocranial anatomy as compared to the domestic goat. The foramen orbitorotundum is round in muskoxen as opposed to a teardrop shape in goats, and the foramen ovale is smaller and more medially located than in goats. The external occipital protuberance is very pronounced in the adult muskox as compared to the neonate and goat, whereas the internal occipital protuberance is less pronounced. The comparison of adult, juvenile, and neonate muskoxen showed that the younger individuals have separate, non-ossified cranial bones and they additionally lack pneumatization, despite it being extensive and characteristic in the adult. While more limited in the juveniles, the adult muskox showed especially prominent endocranial roughness.

4.2 | Endocranial roughness

Our hypothesis was originally that a rough brain cavity could mechanically increase brain stabilization by increasing surface contact area and providing grip through friction. The increased points of contact between the brain and the skull would also distribute force over a broader area, additionally serving to diffract shockwaves incurred by forceful impacts, thus reducing coup-contrecoup injuries that would otherwise lead to concussion. Therefore, the goal of this study was to quantify endocranial roughness by counting the number of endocranial ridges that were visible to the naked eye. Our results indicate that the ERI was not correlated to headbutting behavior. ERI was designed as a simplistic measure that, when combined with the limitations of our sample, was not able to detect the changes we expected at a coarse scale. Nevertheless, the lack of stark differentiation between endocranial roughness in headbutting and non-headbutting bovid species in this study could also be explained by additional factors. Endocranial roughness may affect brain protection only at a smaller scale; or, at the measured scale, endocranial roughness has no effect on protecting the brain during headbutting (at least not one strong enough to cause evolutionary pressure) and therefore the brain cavity is not affected by sexually-selected cranial modifications related to headbutting.

Limitations to our experimental methods should be taken into consideration. As there are few species that truly headbutt, our analysis was affected by a low sample size of headbutting animals and even fewer available CT scans for those species. Thus, our large sample size for non-headbutting animals represents the true relationship of our sample. Figure 4 shows a nonsignificant difference of non-headbutting animals with higher ERI scores. This can be explained by both the low representation of headbutting animals in our sample, as well as a mild trend of voxel size correlating to ERI scores for the larger specimens, meaning that skull size could be a limiting factor in this analysis. We used animal weight as a proxy for skull size, as our samples range from the smallest bovid, the pygmy antelope (2.5 kg) to one of the largest, the bison (700 kg). Skull size (as well as horn length) affects the size of a CT scanner's field of view, increasing voxel size and decreasing scan resolution. Our scoring was likely skewed by the fact that the animals with larger skulls (often those who headbutt the most) could not be scanned in higher quality, thus potentially resulting in less-detailed 3D renderings and lower ERI scores.

Another consideration is that endocranial roughness is related to the degree of gyrencephaly to a certain extent, due to the close proximity of bone and brain during development. Gyrencephaly tends to be increased in animals with social lifestyles involving large, hierarchical groups driven by sexual selection that require greater information-processing capacities (Shultz & Dunbar, 2006). Artiodactyls in particular show a more gyrified cerebral cortex than those of non-artiodactyl species with similar brain mass (Kazu et al., 2014) and very rough brain cavities (Figure 1). In addition, a recent study found that males of the same ruminant species tend to invest in relatively larger weapons while females invest in relatively larger brains, potentially for increased social complexity and/or male assessment by females (Lopez et al., 2024). In addition to gyrencephaly (Striedter, 2005) and sex (Kobayashi et al., 2014), many other factors likely contribute to differences in endocranial appearance, including phylogeny, age (Van Minh & Hamada, 2017), and diet (Grabowski et al., 2023). Factors influencing local variations in bone thickness may also affect endocranial roughness, including physiological responses to stress, hormones, muscle loading, and allometry (Etienne et al., 2021). Over the course of an animal's lifetime bone plasticity can occur in response to mechanical stress or hormonal fluctuation, however, in that case, we would have expected the species with the highest mechanical stress from headbutting to show a significantly different ERI than those sustaining less mechanical stress, which was not the case in our study. Overall, future studies would benefit from larger sample sizes that account for the aforementioned variables. Advances in CT imaging technology would also be beneficial, enabling the acquisition of higher-resolution images of the endocranial surface in large skulls and investigating roughness at higher resolution. Techniques involving 3D-shape analysis of the brain cavity may be able to determine more detailed differences in roughness (De Jager et al., 2022), but their cost and time investments were outside the scope of the current study.

In the context of evolution, an organism "looses" by failing to pass on its genetic material. For the muskox,

sexual selection plays a critical role in reproductive success, as females select males with higher fitness traits, namely the size of their body and horns, and the ability to win headbutting fights with rivals. Headbutting rarely results in death, and while it can result in brain injury, chronic neurodegeneration is not immediately life-threatening. Therefore, protecting the brain from mild injury may not be subject to selective pressure, and thus cranial adaptations may not extend into the braincase. On the other hand, factors that have yet to be discovered might contribute to protecting the brain from damage due to headbutting. In conclusion, the lack of a clear evolutionary signal for endocranial roughness, or at least one detectable by our simple metric, suggests that the relationship between sexual selection, behavior, and brain injury is complex and merits further study.

AUTHOR CONTRIBUTIONS

Nicole L. Ackermans: Conceptualization; data curation; formal analysis; funding acquisition; investigation; methodology; project administration; resources; supervision; validation; visualization; writing – original draft; writing – review and editing. **Joy S. Reidenberg:** Conceptualization; formal analysis; investigation; methodology; supervision; validation; visualization; writing – original draft; writing – review and editing.

ACKNOWLEDGMENTS

The first draft of this manuscript was written during the first COVID-19 lockdown in New York City. I (NLA) feel therefore obligated to thank the healthcare workers, especially those at Mount Sinai Hospital who dedicated themselves to keeping us safe and healthy at the height of the pandemic, while much remained unknown, and while I was stuck at home writing about muskoxen. This manuscript looks very different now, Theseus would be proud. We thank Roland Frey and Guido Fritch of the Leibniz Institute for Zoo and Wildlife Research Berlin for their contribution to the two juvenile muskox CT and MRI scans as well as the golden takin CT scan. We thank Andy Farke for his contribution to a large dataset of bovid CT scans, as well as his team member Eileen Westwig at the American Museum of Natural History, Department of Mammalogy, and the Department of Radiology at the Stony Brook University Medical Center. We thank the veterinarians of Tierpark Berlin and the pathologists of the Leibniz Institute for Zoo and Wildlife Research for their help with the juvenile muskox and taking specimen CT scans. Thank you to Jamie Luce of The Muskox Farm in Alaska for providing information on Muskox behavior. Thank you to my students, Emma Bowie, Breanna Ciemny, Lillian Howe, and Maren McKean of the Ackermans lab for providing endocranial roughness scores. We thank Jonathan Dombrosky for his insight on statistical analysis. Finally, we are grateful to both reviewers for their patience and their comments, which greatly improved this manuscript.

FUNDING INFORMATION

This work was supported by an early mobility postdoctoral fellowship from the Swiss National Science Foundation number P2ZHP3_191255 (NLA).

ORCID

Nicole L. Ackermans https://orcid.org/0000-0001-8336-1888
Joy S. Reidenberg https://orcid.org/0000-0002-4180-7156

REFERENCES

Ackermans, N., Varghese, M., Williams, T., Grimaldi, N., Selmanovic, E., Alipour, A., Balchandani, P., Reidenberg, J., & Hof, P. (2022). Evidence of traumatic brain injury in headbutting bovids. *Acta Neuropathologica*, *144*, 5–26.

Ackermans, N. L. (2023). Neurobiological tradeoffs of headbutting bovids. *Trends in Neurosciences*, *46*, 898–900.

Ackermans, N. L., Reidenberg, J. S., & Tobiansky, D. J. (2024). Introduction to the TBI special issue - title TBD. *The Anatomical Record*. (in prep).

Aguirre, T. G., Fuller, L., Ingrole, A., Seek, T. W., Wheatley, B. B., Steineman, B. D., Donahue, T. L. H., & Donahue, S. W. (2020). Bioinspired material architectures from bighorn sheep horncore velar bone for impact loading applications. *Scientific Reports*, *10*, 1–14.

Blake, J. E., McLean, B. D., & Gunn, A. (1991). Yersiniosis in free-ranging muskoxen on Banks Island, Northwest Territories, Canada. *Journal of Wildlife Diseases*, *27*, 527–533.

Brand, N., Widga, C., & Schubert, B. (2020). *Musk ox measurements: Differentiating the teeth and crania of the fossil woodland musk ox Bootherium from the tundra musk ox Ovibos*. Society of Vertebrate Palaeontology. Online.

Castelló, J. R. (2016). Bovids of the world: Antelopes, gazelles, cattle, goats, sheep, and relatives. In *Bovids of the world*. Princeton University Press.

Clark, W. L. G., Cooper, D., & Zuckerman, S. (1936). The endocranial cast of the chimpanzee. *The Journal of the Anthropological Institute of Great Britain* Ireland:249-268, *66*, 249.

Coltman, D. W., O'Donoghue, P., Jorgenson, J. T., Hogg, J. T., Strobeck, C., & Festa-Bianchet, M. (2003). Undesirable evolutionary consequences of trophy hunting. *Nature*, *426*, 655–658.

Cooper, N., Bond, A. L., Davis, J. L., Portela Miguez, R., Tomsett, L., & Helgen, K. M. (2019). Sex biases in bird and mammal natural history collections. *Proceedings of the Royal Society B*, *286*, 20192025.

Corlatti, L., Caroli, M., Pietrocini, V., & Lovari, S. (2013). Rutting behaviour of territorial and nonterritorial male chamois: Is there a home advantage? *Behavioural Processes*, *92*, 118–124.

Darlington, D. (1957). The convolutional pattern of the brain and endocranial cast in the ferret (*Mustela furo* L.). *Journal of Anatomy*, *91*, 52–60.

De Jager, E. J., Risser, L., Mescam, M., Fonta, C., & Beaudet, A. (2022). Sulci 3D mapping from human cranial endocasts: A

powerful tool to study hominin brain evolution. *Human Brain Mapping*, *43*, 4433–4443.

Emlen, D. J. (2008). The evolution of animal weapons. *Annual Review of Ecology, Evolution, and Systematics*, *39*, 387–413.

Etienne, C., Filippo, A., Cornette, R., & Houssaye, A. (2021). Effect of mass and habitat on the shape of limb long bones: A morpho-functional investigation on Bovidae (Mammalia: Cetartiodactyla). *Journal of Anatomy*, *238*, 886–904.

Farke, A. A. (2008). Frontal sinuses and head-butting in goats: A finite element analysis. *Journal of Experimental Biology*, *211*, 3085–3094.

Farke, A. A. (2010). Evolution and functional morphology of the frontal sinuses in Bovidae (Mammalia: Artiodactyla), and implications for the evolution of cranial pneumaticity. *Zoological Journal of the Linnean Society*, *159*, 988–1014.

Fortelius, M., & Solounias, N. (2000). Functional characterization of ungulate molars using the abrasion-attrition wear gradient: A new method for reconstructing paleodiets. *American Museum Novitates*, *3301*, 1–36.

Frey, R., Gebler, A., & Fritsch, G. (2006). Arctic roars–laryngeal anatomy and vocalization of the muskox (*Ovibos moschatus*, Zimmermann, 1780, Bovidae). *Journal of Zoology*, *268*, 433–448.

Grabowski, M., Kopperud, B. T., Tsuboi, M., & Hansen, T. F. (2023). Both diet and sociality affect primate brain-size evolution. *Systematic Biology*, *72*, 404–418.

Gray, D. R. (1973). Social organization and behavior of muskoxen (Ovibos moschatus) on Bathurst Island, N.W.T. In *Department of Zoology* (p. 212). University of Alberta.

Gunn, A., Miller, F. L., & McLean, B. (1989). Evidence for and possible causes of increased mortality of bull muskoxen during severe winters. *Canadian Journal of Zoology*, *67*, 1106–1111.

Harington, C. (1970). A Pleistocene muskox (*Ovibos moschatus*) from gravels of Illinoian age near Nome, Alaska. *Canadian Journal of Earth Sciences*, *7*, 1326–1331.

Ihl, C., & Bowyer, R. T. (2011). Leadership in mixed-sex groups of muskoxen during the snow-free season. *Journal of Mammalogy*, *92*, 819–827.

International Committee on Veterinary Gross Animal Nomenclature I. (2017). *Nomina Anatomica Veterinaria, sixth edition*. The Editorial Committee of the International Committee on Veterinary Gross Animal Nomenclaure.

Kazu, R. S., Maldonado, J., Mota, B., Manger, P. R., & Herculano-Houzel, S. (2014). Cellular scaling rules for the brain of Artiodactyla include a highly folded cortex with few neurons. *Frontiers in Neuroanatomy*, *8*, 128.

Kitts, D. B. (1953). *A Pleistocene musk ox from New York and the distribution of the musk-oxen*. American Museum Novitates.

Kobayashi, Y., Matsui, T., Haizuka, Y., Ogihara, N., Hirai, N., & Matsumura, G. (2014). Cerebral sulci and gyri observed on macaque Endocasts. In T. Akazawa, N. Ogihara, C. Tanabe, & H. Terashima (Eds.), *Dynamics of learning in Neanderthals and modern humans volume 2: Cognitive and physical perspectives* (pp. 131–137). Springer Japan.

Kopperud, B. T. (2017). Artiodactyl brain-size evolution. A phylogenetic comparative study of brain-size adaptation. In *Centre for ecological and evolutionary synthesis* (p. 69). University of Oslo.

Krakhmalnaya, T. V., & Kovalchuk, O. M. (2018). Fossil *Ovibos Moschatus* (Artiodactyla, Bovidae) from Buryn, with reference to muskox dispersal in the late Pleistocene of Ukraine. *Vestnik Zoologii*, *52*, 463–470.

Lent, P. C. (1988). Ovibos moschatus. *Mammalian species*, *302*, 1–9.

Lönnberg, E. (1901). *Studies on ruminants*. Kungl. boktryckeriet, PA Norstedt & söner.

Lopez, N., Moore Tupas, J., & Stankowich, T. (2024). Brains vs brawn: Relative brain size is sexually dimorphic amongst weapon-bearing ruminants. *Behavioral Ecology and Sociobiology*, *78*, 11.

Lovari, S., & Apollonio, M. (1994). On the rutting behaviour of the Himalayan goral *Nemorhaedus goral* (Hardwicke, 1825). *Journal of Ethology*, *12*, 25–34.

Lovari, S., Mori, E., & Procaccio, E. L. (2020). On the behavioural biology of the mainland serow: A comparative study. *Animals*, *10*, 1669.

Lundrigan, B. (1996). Morphology of horns and fighting behavior in the family Bovidae. *Journal of Mammalogy*, *77*, 462–475.

Márquez, S., Pagano, A. S., Schwartz, J. H., Curtis, A., Delman, B. N., Lawson, W., & Laitman, J. T. (2017). Toward understanding the mammalian zygoma: Insights from comparative anatomy, growth and development, and morphometric analysis. *The Anatomical Record*, *300*, 76–151.

Mathiesen, S., Sørmo, W., Haga, Ø., Norberg, H., Utsi, T., & Tyler, N. (2000). The oral anatomy of Arctic ruminants: Coping with seasonal changes. *Journal of Zoology*, *251*, 119–128.

Opdam, H. I., Federico, P., Jackson, G. D., Buchanan, J., Abbott, D. F., Fabinyi, G. C., Syngeniotis, A., Vosmansky, M., Archer, J. S., & Wellard, R. M. (2002). A sheep model for the study of focal epilepsy with concurrent intracranial EEG and functional MRI. *Epilepsia*, *43*, 779–787.

Peña-Melián, A., Rosas, A., García-Tabernero, A., Bastir, M., & De La Rasilla, M. (2011). Paleoneurology of two new neandertal occipitals from El Sidrón (Asturias, Spain) in the context of *homo* endocranial evolution. *The Anatomical Record: Advances in Integrative Anatomy and Evolutionary Biology*, *294*, 1370–1381.

Pérez-Barbería, F. J., & Gordon, I. J. (2005). Gregariousness increases brain size in ungulates. *Oecologia*, *145*, 41–52.

Picard, K., Thomas, D. W., Festa-Bianchet, M., Belleville, F., & Laneville, A. (1999). Differences in the thermal conductance of tropical and temperate bovid horns. *Ecoscience*, *6*, 148–158.

Picard, K., Thomas, D. W., Festa-Bianchet, M., & Lanthier, C. (1994). Bovid horns: An important site for heat loss during winter? *Journal of Mammalogy*, *75*, 710–713.

Preuschoft, H., & Witzel, U. (2002). Biomechanical investigations on the skulls of reptiles and mammals. *Senckenbergiana Lethaea*, *82*, 207–222.

R Core Team. (2021). *R: A language environment for statistical computing. 4.3.1*. R Foundation for Statistical Computing.

Schaller, O., & Constantinescu, G. M. (2007). *Illustrated veterinary anatomical nomenclature, Illustrated ed*. Georg Thieme Verlag.

Schüler, S., Sharp, A. C., & Nyakatura, J. A. (2024). Comparative finite element analysis of the first thoracic vertebra in artiodactyls. *Journal of Morphology*, *285*, e21695.

Shultz, S., & Dunbar, R. I. M. (2006). Both social and ecological factors predict ungulate brain size. *Proceedings of the Royal Society B: Biological Sciences*, *273*, 207–215.

Skwarawoolf, T., & Millar, J. F. V. (1981). Pleistocene muskox (*Ovibos moschatus*) from near Saskatoon, Saskatchewan. *Canadian Journal of Earth Sciences*, *18*, 852–857.

Smith, P. A., Schaefer, J. A., & Patterson, B. R. (2002). Variation at high latitudes: The geography of body size and cranial

morphology of the muskox, *Ovibos moschatus*. *Journal of Biogeography*, *29*, 1089–1094.

Smith, T. (2008). Muskox: Alaska Department of Fish and Game wildlife notebook. Alaska.

Smith, T. E. (1976). Reproductive behavior and related social organization of the muskox on Nunivak Island. In *Life Sciences* (p. 138). University of Alaska Fairbanks.

Snively, E., & Theodor, J. M. (2011). Common functional correlates of head-strike behavior in the pachycephalosaur *Stegoceras validum* (Ornithischia, Dinosauria) and combative artiodactyls. *PLoS One*, *6*, e21422.

Stefaniak, K., Lipecki, G., Nadachowski, A., Semba, A., Ratajczak, U., Kotowski, A., Roblíčková, M., Wojtal, P., Shpansky, A. V., & Malikov, D. G. (2021). Diversity of muskox *Ovibos moschatus* (Zimmerman, 1780) (Bovidae, Mammalia) in time and space based on cranial morphometry. *Historical Biology*, *33*, 62–77.

Striedter, G. F. (2005). *Principles of brain evolution*. Sinauer Associates.

Taylor, C. R. (1966). The vascularity and possible thermoregulatory function of the horns in goats. *Physiological Zoology*, *39*, 127–139.

Thing, H., Klein, D., Jingfors, K., & Holt, S. (1987). Ecology of muskoxen in Jameson land, northeast Greenland. *Ecography*, *10*, 95–103.

Van Minh, N., & Hamada, Y. (2017). Age-related changes of sulcal imprints on the endocranium in the Japanese macaque (*Macaca fuscata*). *American Journal of Physical Anthropology*, *163*, 285–294.

Vander Linden, A., & Dumont, E. R. (2019). Intraspecific male combat behaviour predicts morphology of cervical vertebrae in ruminant mammals. *Proceedings of the Royal Society B*, *286*, 20192199.

Walker, D. N. (1982). A late Pleistocene *Ovibos* from southeastern Wyoming. *Journal of Paleontology*, *56*, 486–491.

Wheatley, B. B., Gilmore, E. C., Fuller, L. H., Drake, A. M., & Donahue, S. W. (2023). How the geometry and mechanics of bighorn sheep horns mitigate the effects of impact and reduce the head injury criterion. *Bioinspiration & Biomimetics*, *18*, 026005.

Wilkinson, P. F., & Shank, C. C. (1976). Rutting-fight mortality among musk oxen on Banks Island, Northwest Territories, Canada. *Animal Behaviour*, *24*, 756–758.

Woodruff, D. C., & Ackermans, N. L. (2024). Headbutting through time: A review of this hypothesized behavior in "dome-headed" fossil taxa. *The Anatomical Record*.

Zollikofer, C. P. E., & De León, M. S. P. (2013). Pandora's growing box: Inferring the evolution and development of hominin brains from endocasts. *Evolutionary Anthropology: Issues, News, and Reviews*, *22*, 20–33.

SUPPORTING INFORMATION

Additional supporting information can be found online in the Supporting Information section at the end of this article.

How to cite this article: Ackermans, N. L., & Reidenberg, J. S. (2025). Only skull-deep? Headbutting adaptations may not extend to the brain cavity. *The Anatomical Record*, 1–13. https://doi.org/10.1002/ar.25623